Active/Reactive Power Control of Photovoltaic Grid-Tied Inverters with Peak Current Limitation and Zero Active Power Oscillation during Unbalanced Voltage Sags

Dehghani Tafti, Hossein; Maswood, Ali Iftekhar; Konstantinou, Georgios; Pou, Josep; Acuña, Pablo

2018

Dehghani Tafti, H., Maswood, A. I., Konstantinou, G., Pou, J., & Acuña, P. (2018). Active/Reactive Power Control of Photovoltaic Grid-Tied Inverters with Peak Current Limitation and Zero Active Power Oscillation during Unbalanced Voltage Sags. IET Power Electronics, 11(6), 1066-1073.

https://hdl.handle.net/10356/87442

https://doi.org/10.1049/iet-pel.2017.0210

Active/Reactive Power Control of Photovoltaic Grid-Tied Inverters with Peak Current Limitation and Zero Active Power Oscillation during Unbalanced Voltage Sags

Hossein Dehghani Tafti[1,*], Ali Iftekhar Maswood[1], Georgios Konstantinou[2], Josep Pou[1], Pablo Acuna[2]

[1]School of Electrical and Electronic Engineering, Nanyang Technological University, 50 Nanyang Ave, Singapore
[2]School of Electrical Engineering and Telecommunications, University of New South Wales, Sydney, NSW, 2052, Australia
[*]hossein002@e.ntu.edu.sg

Abstract: This paper proposes an analytical expression for the calculation of active and reactive power references of a grid-tied inverter, which limits the peak current of the inverter during voltage sags. The key novelty is that the active/reactive power references are analytically calculated based on the dc-link voltage and grid codes, while they do not depend on the implemented current reference calculation algorithm and, as a general formulation, can be implemented in combination with various current reference calculation algorithms. Furthermore, based on the inverter nominal current and the injected reactive power to the grid during voltage sags, an analytical algorithm is introduced for the calculation of the active power reference, which can be extracted from PV strings. The proposed algorithm ensures that the maximum current capability of the inverter is used for the enhancement of the grid voltages during voltage sags, while it always complies with the reactive power injection requirement of grid codes and avoids increasing the dc-link voltage excessively. An unbalanced current injection algorithm is also applied for the grid-tied inverter which results in zero active power oscillation. Experimental results of a grid-connected 3.3-kVA, three-level, neutral-point-clamped inverter laboratory prototype under several voltage sag conditions are presented to demonstrate the effectiveness of the proposed controller.

1. Introduction

High penetration of distributed generation (DG) units in the power system has resulted in new electricity regulation requirements, particularly during grid voltage sags. Initially, low-voltage ride-through (LVRT) capability was introduced by power system operators in order to withstand voltage sags and maintain the connection to the grid and avoid loss of power generation [1,2]. Later, reactive power injection was added in grid codes with the intention of supporting the grid voltage and reducing the possibility of voltage collapse during network faults. Furthermore, negative-sequence current injection appears to be a new important requirement of next generation of grid codes for enhancing the DG capabilities in supporting unbalanced voltage sags [3].

Among various DG units, grid-connected photovoltaic power plants (GCPVPPs) have recently achieved a drastic increase in the installed capacity due to the decreased module prices and favorable incentive policies [4]. As a result, LVRT became a necessary requirement for medium-

and large-scale GCPVPPs. Several studies have been performed on LVRT capability of single- and two-stage GCPVPPs considering the injection of balanced active/reactive currents to the grid during voltage sags [5–7].

Unbalanced voltage sags are more common in power systems, causing several adverse effects including overloading of distribution transformers, higher losses and lower stability of the power system. The negative-sequence component of the voltage results in double fundamental frequency oscillation of the injected active or reactive power to the grid. On the other hand, injection of balanced reactive currents during unbalanced grid voltage sags, may result in overvoltage of nonfaulty phases [8–10]. Therefore, the design of the controller of the grid-connected inverter becomes more challenging during unbalanced grid voltage sags.

Various flexible active power injection algorithms have been implemented in [11, 12] with the ability to minimize oscillations of either active or reactive power during unbalanced voltage sags. However, injection of reactive power during voltage sags can be more beneficial in voltage enhancement of point of common coupling (PCC) [8]. A number of studies have been carried out on flexible active/reactive power injection to the grid during unbalanced voltage sags with various control aims such as oscillating power control [10, 13], grid voltage support [8], maximizing inverter power capability [14] and in-phase current compensation [15].

The peak current limitation during voltage sags is taken into consideration in few studies [3, 16–21]. The active power injection is considered in [16], while the reactive power injection is studied in [18]. Several control strategies are also introduced in [20], however few of them satisfy the peak current limitation. The active and reactive power injection with peak current limitation is investigated in [21], however only positive sequence current injection is applied. Finally, an active/reactive positive/negative sequence power injection method with peak current limitation is investigated in [3], where the amount of injected reactive power is calculated based on the injected active power and nominal current of the inverter. The injection of the active power is given priority to the reactive power in [3], although based on the grid codes and standards [2], during voltage sags, the injection of the reactive power should be given priority to the active power.

This paper derives an analytical expression for calculating active/reactive power references (P^* and Q^*) which limits the inverter peak current during voltage sags. Unlike the current studies in the literature [3, 16–18, 20, 21], the proposed analytical expression for P^* and Q^* does not depend on the current reference calculation method and, as a general formulation, can be implemented in combination with various such methods. Additionally, an analytical expression is introduced which calculates the required active power from PV strings during voltage sags. This method ensures that the inverter current remains within its nominal operation range and also keeps the dc-link voltage at its nominal value. The proposed power references are used to define improved current references, which result in zero active power oscillation. In order to obtain a constant dc-link voltage and maintain the active and reactive power injection during voltage sags, a coordinated maximum power point tracking (MPPT) algorithm is also implemented for the dc-dc converters of the multi-string GCPVPP, which reduces the extracted power from PV strings to the amount of active power that can be injected to the grid according to the inverter nominal current and the injected reactive current.

The rest of the paper is organized as follows. Section 2 provides an overview of the GCPVPP structure, while principles of unbalanced active/reactive power theory are discussed in Section 3. The detailed implementations of the voltage sag detector, proposed active/reactive power and current reference calculation algorithm, current controller and dc-dc converter controller during voltage sags are described in Section 4. Experimental results of the proposed controller on a

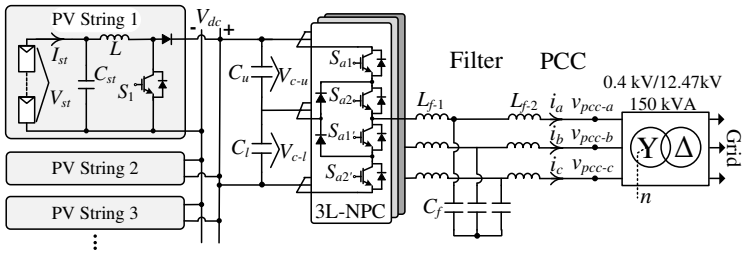

Fig. 1. *Grid-connected PV power plant structure.*

3.3-kVA laboratory three-level neutral-point-clamped (3L-NPC) inverter are illustrated in Section 5 and the conclusions of the work are summarized in Section 6.

2. Multi-String PV Power Plant Configuration

The multi-string two-stage GCPVPP structure, depicted in Fig. 1, is among state-of-the-art configurations for medium- and large-scale GCPVPPs, because of its several advantages [22–24]:

- The extraction of maximum power from all of the PV strings during partial shading and mismatch between PV panels.
- Ability to extract power from PV strings during sunrise/sunset or cloudy sky with low irradiation.
- Higher modularity compared to the single-stage power conversion with a central inverter.
- Elimination of low frequency bulky transformer when isolated dc-dc converters with high frequency transformer are used.
- Simpler structure and control algorithms compared to the single-stage power conversion structure with micro-inverters.

It consists of multiple PV strings, dc-dc converters and a central grid-connected inverter. In this study, a dc-dc boost converter is used in each PV string and a 3L-NPC inverter is utilized for the connection of the GCPVPP to the grid. The YΔ transformer steps up the output voltage of the inverter to the grid voltage. It also provides electrical isolation between the grid and GCPVPP, which eliminates possible earth leakage currents in the grid and ensures standard safety requirements. The LCL filter, connected between the inverter and grid, aids in improving the total harmonic distortion performance in order to comply with grid codes and standards, e.g. IEEE standard 1547 [25].

3. Principles of Unbalanced Active/Reactive Power Theory

According to the instantaneous power theory, the injected active power (p) to the grid for GCPVPP, shown in Fig.1, is:

$$p = v_{pcc} i_{abc} = v_{pcc\text{-}a} i_a + v_{pcc\text{-}b} i_b + v_{pcc\text{-}c} i_c, \tag{1}$$

where $v_{pcc} = [v_{pcc\text{-}a}\ v_{pcc\text{-}b}\ v_{pcc\text{-}c}]$ are the phase-neutral voltages of PCC and $i_{abc} = [i_a\ i_b\ i_c]^T$ are the output currents of the grid-connected 3L-NPC inverter, shown in Fig. 1.

The instantaneous active power can be calculated using the symmetric sequence transformation as follows:

$$\begin{aligned} p &= (v_{pcc}^{+} + v_{pcc}^{-}).(i_{abc}^{+} + i_{abc}^{-}) \\ &= \left(\overbrace{v_{pcc}^{+} i_{abc}^{+}}^{P^{+}} + \overbrace{v_{pcc}^{-} i_{abc}^{-}}^{P^{-}}\right) + \left(\overbrace{v_{pcc}^{+} i_{abc}^{-} + v_{pcc}^{-} i_{abc}^{+}}^{\tilde{p}}\right) \\ &= P + \tilde{p}, \end{aligned} \tag{2}$$

where v_{pcc}^{+} and v_{pcc}^{-} are the three-phase PCC positive- and negative-sequence voltage vectors, while i_{abc}^{+} and i_{abc}^{-} are the inverter positive- and negative-sequence current vectors. P is the average active power and $\tilde{p}$ is its oscillatory term. Accordingly, P^{+} and P^{-} are the positive- and negative-sequences of the average active power, respectively.

A traditional algorithm to compute the current references is to define values k_1 and k_2 as the ratio of the positive-sequence active or reactive power to the total active or reactive power ($k_1 = \dfrac{P^{+}}{P}$ and $k_2 = \dfrac{Q^{+}}{Q}$), where Q is the average reactive power and Q^{+} is its positive-sequence [15]. Hence, the current references can be calculated as follows:

$$\begin{aligned} i_{abc}^{*} = &\overbrace{\frac{k_1 P^{*}}{\mid v_{pcc}^{+} \mid^2} v_{pcc}^{+}}^{i_{abc\text{-}p}^{+}} + \overbrace{\frac{(1-k_1) P^{*}}{\mid v_{pcc}^{-} \mid^2} v_{pcc}^{-}}^{i_{abc\text{-}p}^{-}} \\ &+ \overbrace{\frac{k_2 Q^{*}}{\mid v_{pcc}^{+} \mid^2} v_{pcc\perp}^{+}}^{i_{abc\text{-}q}^{+}} + \overbrace{\frac{(1-k_2) Q^{*}}{\mid v_{pcc}^{-} \mid^2} v_{pcc\perp}^{-}}^{i_{abc\text{-}q}^{-}}, \end{aligned} \tag{3}$$

with

$$v_{pcc\perp} = \frac{1}{\sqrt{3}} \begin{bmatrix} 0 & 1 & -1 \\ -1 & 0 & 1 \\ 1 & -1 & 0 \end{bmatrix} v_{pcc},$$

where P^{*} and Q^{*} are the average active and reactive power references. Thus, the positive- and negative-sequences of the current reference can be computed according to (3) as:

$$i_{abc}^{+^{*}} = \frac{k_1 P^{*} - \boldsymbol{j} k_2 Q^{*}}{\mid v_{pcc}^{+} \mid^2} v_{pcc}^{+} \tag{4}$$

$$i_{abc}^{-^{*}} = \frac{(1-k_1) P^{*} + \boldsymbol{j}(1-k_2) Q^{*}}{\mid v_{pcc}^{-} \mid^2} v_{pcc}^{-}. \tag{5}$$

It is shown that the positive- and negative-sequences of the current reference depend on k_1 and k_2. Therefore, as will be explained later in detail, these values can be instantaneously calculated based on the purpose of the controller during unbalanced voltage sags.

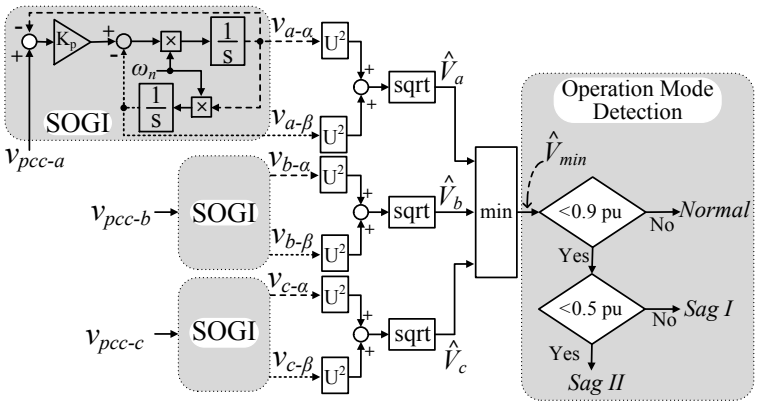

Fig. 2. *Voltage sag detection algorithm.*

4. Proposed Active/Reactive Power Controller during Unbalanced Voltage Sags

Two separate controllers for the grid-connected 3L-NPC inverter and the dc-dc converters are required to operate the GCPVPP system. These controllers along with the proposed algorithms for calculation of the active/reactive power references and current references are presented in detail in the following subsections. Each of these controllers require separate control strategies, which are specific for a GCPVPP operation mode. Therefore, a fast and precise voltage disturbance detection algorithm is required to determine the operating mode of the GCPVPP. The voltage sag detection algorithm, used in this work, is presented in the following subsection.

4.1. Voltage Sag Detector

Fast detection of the voltage sag is important for quick operation of the controller at the beginning of the voltage sag. In this study, second order generalized integrator (SOGI) based orthogonal system is applied for the calculation of the amplitude of phase voltages, as illustrated in Fig. 2. Since the phase voltage amplitudes are required to detect the single- or two-phase voltage sags, the orthogonal voltages ($v_{x\text{-}\alpha}$ and $v_{x\text{-}\beta}$, where x is referred to phase a, b or c) are calculated by independent SOGI blocks for each phase. In this figure, ω_n denotes the fundamental angular frequency of the grid voltage. The amplitude of the phase voltage ($\hat{V}_x$) is calculated as:

$$\hat{V}_x = \sqrt{v_{x\text{-}\alpha}^2 + v_{x\text{-}\beta}^2}. \tag{6}$$

Subsequently, the minimum voltage amplitude ($\hat{V}_{min}$) is determined dynamically by the controller, which is utilized for the detection of the voltage sag and operation mode.

The requirement of grid codes for the reactive current injection of medium- and large-scale GCPVPPs is [2]:

$$I_q^* = \begin{cases} 0, & 0.9\,\text{pu} \le \hat{V}_{min} < 1.1\,\text{pu} \\ k\dfrac{\Delta V}{\hat{V}_N} I_{N_{dq}} + I_{q0}, & 0.5\,\text{pu} \le \hat{V}_{min} < 0.9\,\text{pu} \\ -I_{N_{dq}} + I_{q0}, & \hat{V}_{min} < 0.5\,\text{pu}, \end{cases} \tag{7}$$

where $\hat{V}_N$ is the nominal amplitude of the PCC phase voltage and $\Delta V = \hat{V}_{min} - \hat{V}_N$. It should be noted that $\hat{V}_{min}$ is calculated dynamically by the controller. $I_{N_{dq}}$ denotes the transformed inverter nominal current to the dq-coordinate ($I_{N_{dq}} = \sqrt{3} I_N$, where I_N is the nominal rms current of the inverter), based on the implemented transformation coefficients. I_{q0} is the initial reactive current of the inverter before the voltage sag. k is a constant value defined according to the agreement between power system operator and power producer and is usually larger or equal to 2 [2]. In this study, k is considered to be 2.

Since three different operating conditions are defined by the grid codes, the proposed controller also is divided into three modes as shown in Fig. 2. If $\hat{V}_{min}$ is between $0.9\,\mathrm{pu}$ and $1.1\,\mathrm{pu}$, the controller operates normally (*Normal*). If $\hat{V}_{min}$ is between $0.5\,\mathrm{pu}$ and $0.9\,\mathrm{pu}$, the inverter is required to inject both active and reactive power to the grid simultaneously (*Sag I*). Finally, when $\hat{V}_{min}$ is smaller than $0.5\,\mathrm{pu}$, the inverter should inject only reactive current to the grid (*Sag II*).

4.2. Proposed Active/Reactive Power Reference Calculation Algorithm

The controller of the 3L-NPC inverter is used to maintain the dc-link voltage (V_{dc}) by controlling the injected active power into the grid. It is realized by manipulating the d-axis current reference (I_d^*) through a PI controller. The q-axis current reference (I_q^*) is calculated from the grid code as in (7). In order to achieve unity power factor operation during *Normal* operation mode, I_q^* is set to zero.

According to (4) and (5), the average active and reactive power references (P^* and Q^*) are required for the calculation of unbalanced current references. On the other hand, the dc-link voltage controller and grid codes provide the d-axis and q-axis current references (I_d^* and I_q^*). Consequently, the instantaneous calculation of P^* and Q^* from I_d^* and I_q^* is necessary for the operation of GCPVPP during various operation modes.

In dq frame, the amount of injected active and reactive power can be calculated as:

$$p = v_d i_d + v_q i_q \tag{8}$$

$$q = v_q i_d - v_d i_q, \tag{9}$$

where v_d and v_q are the instantaneous d-axis and q-axis components of PCC voltage and i_d and i_q denote the instantaneous components of the injected current to the grid. Accordingly, the average injected active and reactive powers can be calculated as:

$$P = \frac{1}{T_w} \Big| \int_{t-T_w}^{t} v_d i_d dt + \int_{t-T_w}^{t} v_q i_q dt \Big| \tag{10}$$

$$Q = \frac{1}{T_w} \Big| \int_{t-T_w}^{t} v_q i_d dt - \int_{t-T_w}^{t} v_d i_q dt \Big|, \tag{11}$$

where P and Q are the average active and reactive powers, respectively. T_w is the window width used for the average calculation, typically $T/2$ or T, T being the grid-voltage period ($T = 1/f$, where f is the grid voltage fundamental frequency). i_d and i_q are calculated with the outer control loop and it can be assumed that their values remain constant within one average calculation window

width, being equal to I_d and I_q, respectively. Consequently, the average active and reactive powers can be written as:

$$P = \frac{1}{T_w}\Big|I_d \int_{t-T_w}^{t} v_d dt + I_q \int_{t-T_w}^{t} v_q dt\Big| \tag{12}$$

$$Q = \frac{1}{T_w}\Big|I_d \int_{t-T_w}^{t} v_q dt - I_q \int_{t-T_w}^{t} v_d dt\Big|. \tag{13}$$

The voltage vector can be represented in dq coordinates through the Park transformation using a synchronous reference frame rotating at the fundamental frequency [26]:

$$\begin{bmatrix} v_d \\ v_q \end{bmatrix} = \mid v^{+}_{pcc_1} \mid \begin{bmatrix} \cos(\theta_0) \\ \sin(\theta_0) \end{bmatrix} + \sum_{\substack{n=-\infty \\ n\neq 1}}^{\infty} \mid v^{+}_{pcc_n} \mid \begin{bmatrix} \cos[(n-1)\omega t + \theta_0 + \theta_n] \\ \sin[(n-1)\omega t + \theta_0 + \theta_n] \end{bmatrix} \tag{14}$$

where the angle θ_0 corresponds to the initial position of the d-axis in the dq transformation and n refers to the harmonic number. $|v^{+}_{pcc_1}|$ is the amplitude of positive-sequence fundamental voltage which in this study is referred as $|v^{+}_{pcc}|$. Assuming that d-axis is aligned with the voltage vector, then $\theta_0 = 0$. Accordingly, the average dq-axis voltages can be calculated, by integrating from (14), as below:

$$V_d = \frac{1}{T_w}\int_{t-T_w}^{t} v_d dt = \mid v^{+}_{pcc} \mid \tag{15}$$

$$V_q = \frac{1}{T_w}\int_{t-T_w}^{t} v_q dt = 0, \tag{16}$$

where V_d and V_q are the average values of v_d and v_q during one average calculation window width. The integral of harmonics in (14) over one voltage cycle equals to zero.

By inserting (15) and (16) in (12) and (13), the average active and reactive power references are calculated as:

$$P = \mid I_d \mid . \mid v^{+}_{pcc} \mid \tag{17}$$

$$Q = \mid I_q \mid . \mid v^{+}_{pcc} \mid . \tag{18}$$

The equations (17) and (18) are applied in the proposed controller for computing the active and reactive power reference as:

$$P^* = \mid I^*_d \mid . \mid v^{+}_{pcc} \mid \tag{19}$$

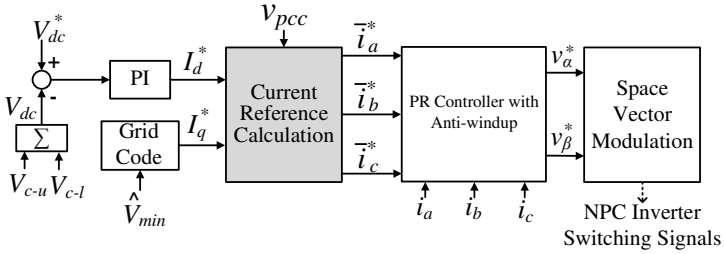

Fig. 3. *Current control strategy for the grid-connected 3L-NPC inverter.*

$$Q^* = \mid I_q^* \mid . \mid v_{pcc}^+ \mid, \tag{20}$$

where I_d^* and I_q^* are calculated from the dc-link voltage controller and the grid code. $\mid v_{pcc}^+ \mid$ is instantaneously calculated from PCC phase voltages as depicted in Fig. 3. Finally, the active/reactive power references (19) and (20) are used in (4) and (5) in order to calculate the current references. In the proposed algorithm, the amount of active/reactive power does not depend on the current reference calculation algorithm, and (19) and (20) are general equations that can be implemented in combination with various current reference calculation methods, while the peak current of the inverter during voltage sags remains within its nominal value.

4.3. Proposed Unbalanced Current Reference Calculation Algorithm with Zero Active Power Oscillation

After calculating the active/reactive power references, the unbalanced current references are calculated in order to obtain zero active power oscillation of GCPVPP during unbalanced voltage sags because:

- Injecting high amount of reactive current to the nonfaulty phases during unbalanced voltage sags, may result in over voltages. Therefore, the amount of injected reactive current to the nonfaulty phases should be smaller than of the faulty ones. This means that the amplitude of the injected current to each phase should be in reverse proportion to its voltage amplitude, which as a result, the instantaneous active power remains constant over the time.
- The oscillation of the active power results in second-order harmonic oscillation of the dc-link voltage. Therefore, the injected active power oscillation should be reduced to zero in order to minimize the dc-link voltage oscillation while avoiding unnecessary trips on dc-voltage protections.

The active power oscillation can be calculated by substituting the positive- and negative-sequence currents from (4) and (5) in (2), as follows:

$$\begin{aligned}\tilde{p} = &\left[\left(\frac{1-k_1}{\mid v_{pcc}^- \mid^2} + \frac{k_1}{\mid v_{pcc}^+ \mid^2}\right)P^* \right.\\ &\left. + \boldsymbol{j}\left(\frac{1-k_2}{\mid v_{pcc}^- \mid^2} - \frac{k_2}{\mid v_{pcc}^+ \mid^2}\right)Q^*\right] v_{pcc}^+ . v_{pcc}^-.\end{aligned} \tag{21}$$

Since the target is to obtain positive and negative sequences of the current references while obtaining zero active power oscillation, k_1 and k_2 are obtained from (21), considering $\tilde{p}$ equal to

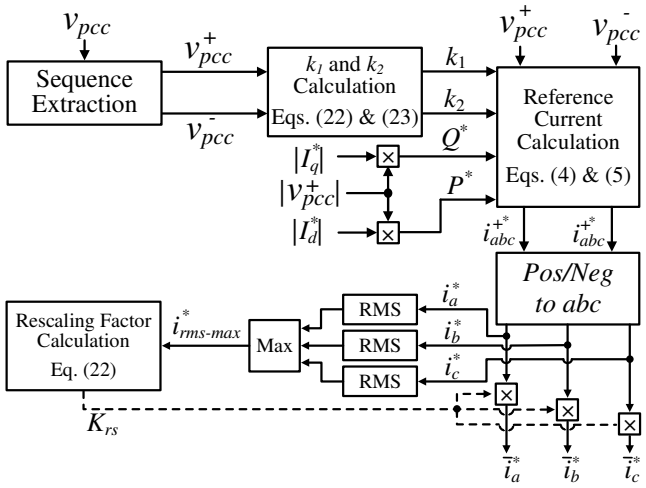

Fig. 4. *Proposed current reference calculation algorithm during unbalanced voltage sags.*

zero, as per:

$$k_1 = \frac{1}{1 - \frac{|\, v_{pcc}^{-} \,|^2}{|\, v_{pcc}^{+} \,|^2}} \tag{22}$$

$$k_2 = \frac{1}{1 + \frac{|\, v_{pcc}^{-} \,|^2}{|\, v_{pcc}^{+} \,|^2}}. \tag{23}$$

Then, k_1 and k_2, which change dynamically based on the instantaneous grid positive- and negative-sequence voltages, are used for the calculation of the current references ((4) and (5)). This ensures zero oscillation of the injected active power of the inverter during all operation modes.

4.4. Current Control Strategy during Unbalanced Voltage Sags

A comprehensive schematic of the proposed current controller is illustrated in Fig. 3. After calculating I_d^* and I_q^*, the phase current references ($\bar{i}_a^*$, $\bar{i}_b^*$ and $\bar{i}_c^*$) are calculated based on the grid voltages. A detailed implementation of the proposed current reference calculation algorithm is shown in Fig. 4. Firstly, the PCC positive- and negative-sequence voltages (v_{pcc}^{+} and v_{pcc}^{-}) are calculated. The calculations are implemented in the abc-frame and voltage angle is calculated using the three phase adaptive phase-locked-loop [27]. The positive-sequence voltage is assumed to be aligned with the voltage vector of phase a. As the aim of the controller is to achieve zero active power oscillation during unbalanced voltage sags, k_1 and k_2 are calculated according to (22) and (23). These values are considered in (4) and (5) for the enumeration of positive and negative-sequence current references.

The calculated active and reactive power references from (19) and (20) are considered in the proposed control strategy, as shown in Fig. 4. The positive- and negative-sequence current references are calculated from (4) and (5) and then are transformed to the abc-frame, in order to achieve abc current references.

The calculated current references (i_a^*, i_b^* and i_c^*) of one or two phases may be higher than the inverter nominal current because the controller aims to achieve zero active power oscillation. Thus, the current references should be limited to the inverter nominal current. On the other hand, according to (1), the current references of all three phases should be rescaled with the same factor to ensure the constant active power injection. Therefore, a rescaling factor (K_{rs}) is defined based on the maximum rms value of current references as below:

$$K_{rs} = \begin{cases} \dfrac{I_{rms}}{i^*_{rms\text{-}max}}, & \text{if } i^*_{rms\text{-}max} > I_{rms} \\ 1, & \text{if } i^*_{rms\text{-}max} \leq I_{rms}, \end{cases} \tag{24}$$

where I_{rms} is the rms value of the nominal current of the inverter and $i^*_{rms\text{-}max}$ is the maximum rms value of the three phase current references (Fig. 4). The final current references are calculated as follows:

$$\begin{bmatrix} \bar{i}_a^* \\ \bar{i}_b^* \\ \bar{i}_c^* \end{bmatrix} = K_{rs} \begin{bmatrix} i_a^* \\ i_b^* \\ i_c^* \end{bmatrix}. \tag{25}$$

The errors between the calculated current references and instantaneous phase currents are fed into the proportional resonant (PR) with anti-windup controller which is implemented in the $\alpha\beta$-frame. Although, the implementation of the conventional PI controller for balanced current injection is simple, it requires multiple frame transformation and results in slow performance. On the other hand, for injection of proper unbalanced currents under unbalanced voltage sags, the calculation of both positive- and negative-sequence voltages in dq frame is required which increases the computational complexity [28]. The PR controller with anti-windup shows faster dynamic response and zero steady-state error [29]. Finally, adaptive space vector modulation (SVM) is applied for generating the switching signals of the 3L-NPC inverter, based on [30, 31].

4.5. dc-dc Converter Controller during Voltage Sags

During *Normal* operation, the dc-dc converters of the multi-string GCPVPP (Fig. 1) extract the maximum power from PV strings. However, during *Sag I* or *Sag II*, the extracted power from the PV strings should be reduced due to the current limitation of the inverter. Therefore, a modification in the controller of the dc-dc converters is necessary. A comprehensive schematic of the proposed control algorithm for the dc-dc converters is depicted in Fig. 5. The proposed control algorithm consists of three operation modes:

Normal operation All of the dc-dc converters extract the maximum power from PV strings, which is referred as *MPPT* in this paper. The PV string operates at Point *A* as shown in Fig. 6(a). As illustrated in Fig. 6(b), the calculated V_{MPP} from MPPT algorithm is compared with the instantaneous string voltage (V_{st}) and the error is fed into the PI controller. During this operation mode, the reduction power signal (RP), which will be explained later in this paper, equals zero. Subsequently, the switching signals of the dc-dc boost converter are generated.

Sag I Both active and reactive powers are injected to the grid during this operation state. Priority is given to the reactive power. Firstly, the required reactive current is calculated according to (7).

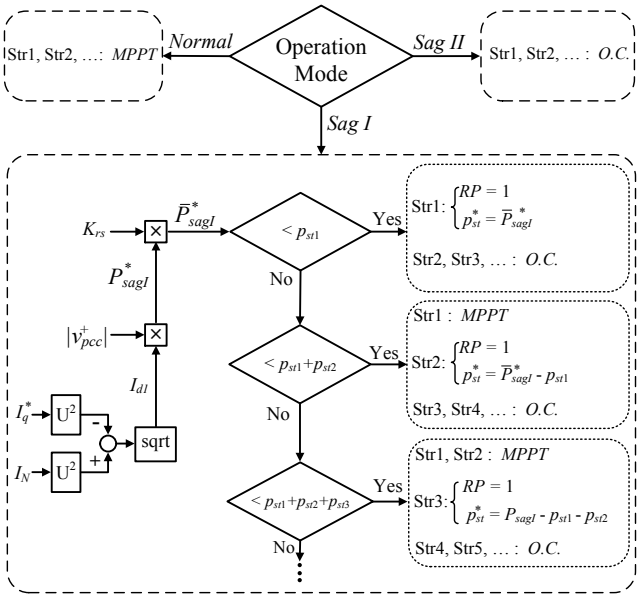

Fig. 5. *Proposed PV strings control algorithm.*

Afterwards, the possible injected active current is calculated based on the nominal current of the inverter as follows:

$$I_{d1} = \sqrt{I^2_{N_{dq}} - I^{*^2}_q}. \tag{26}$$

Subsequently, the maximum possible active power is calculated by (17) based on the maximum possible active current and the amplitude of positive-sequence voltage:

$$P^*_{sagI} = \mid V^+_{pcc} \mid I_{d1}. \tag{27}$$

In order to ensure that the grid code requirement is fulfilled by prioritizing the injected reactive power, the rescaling factor (K_{rs}), is multiplied by the calculated active power reference from (27):

$$\overline{P}^*_{sagI} = K_{rs} P^*_{sagI}. \tag{28}$$

As a result, if the calculated current reference of the 3L-NPC inverter is larger than its nominal current, the controller reduces the active power to give the priority to the reactive power requirement. The active power reference ($\overline{P}^*_{sagI}$) is then compared with extracted power from individual PV strings as depicted in Fig. 5. If $\overline{P}^*_{sagI}$ is smaller than the extracted power of String 1 (p_{st1}), then all other PV strings are open-circuited (*O.C.*) and p_{st1} is reduced to $\overline{P}^*_{sagI}$. This means that the operation point of PV String 1, which is referred as Str1 in Fig. 5, should be moved to Point *B* in Fig. 6. The movement of the operation point from Point *A* to Point *B* during voltage sags is implemented based on the proposed method in [32].

If $\overline{P}^*_{SagI}$ is larger than p_{st1} and is smaller than $p_{st1} + p_{st2}$, the PV String 1 is set to *MPPT*, String 2 operates at power reduction mode ($RP = 1$) and all other PV strings are open circuited. The power reduction algorithm can be implemented in the same manner for other power references (larger than $p_{st1} + p_{st2}$) as well. It should be noted at each moment, only one of PV strings operates at power reduction mode and other PV strings are operating at *MPPT* or *O.C.*. This algorithm results in fast performance of the controller at the beginning of the voltage sag as well as after the clearance of the voltage sag.

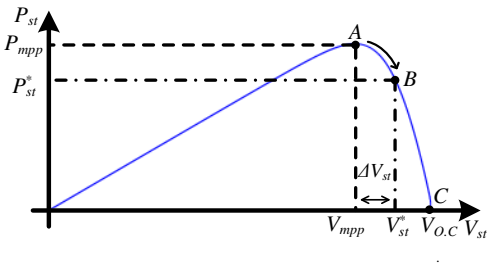

Fig. 6. *Operation point of the PV string on the power-voltage curve during voltage sags.*

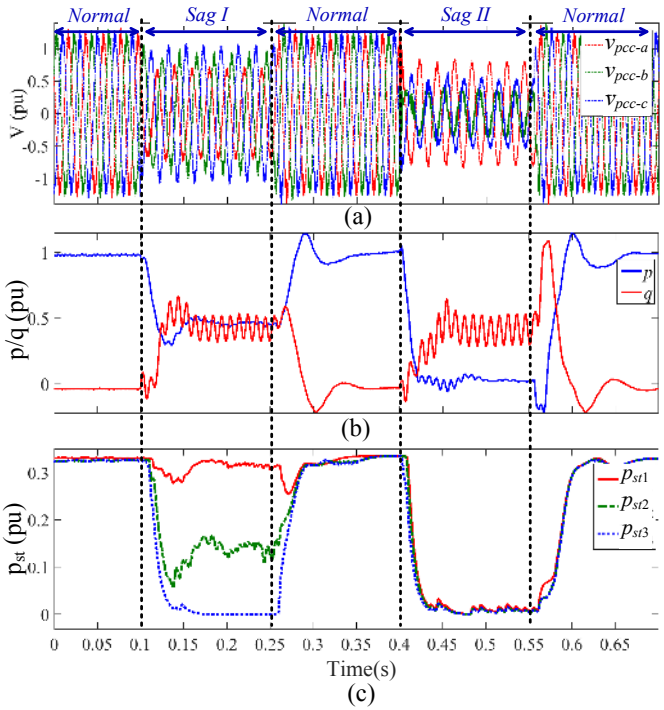

Fig. 7. *Simulation results of multi-string GCPVPP with three PV string during various operation modes: (a) PCC voltages, (b) injected active and reactive power to the grid and (c) extracted power from PV stings.*

Sag II Based on the grid codes, the injected active power to the grid is zero. Therefore, all PV strings are *O.C.* to reduce the extracted power from all PV strings to zero. The dc-link voltage controller, shown in Fig. 3, continues its operation during this operation mode in order to regulate the dc–link voltage to its reference. It should be mentioned that the amount of I^*_d is near zero during *Sag II*, because the extracted power for PV strings is zero. The operation point of the PV sting is moved to point *C* in Fig. 6(a), which results in zero power extraction from the PV string.

The performance of the dc-dc control algorithm is illustrated in Fig. 7. During *Normal* operation, all PV strings operate in *MPPT* mode. The injected active power is $1\,\mathrm{pu}$ and accordingly the extracted power from each one the three PV strings is $0.33\,\mathrm{pu}$. During *Sag I*, the injected active power is reduced to $0.5\,\mathrm{pu}$. Therefore, String 1 remains at *MPPT*, String 3 is *O.C.* and the extracted power of String 2 is reduced to adjust the required active power ($p^*_{st2} = \overline{P}^*_{sagI} - p_{st1}$). During *Sag*

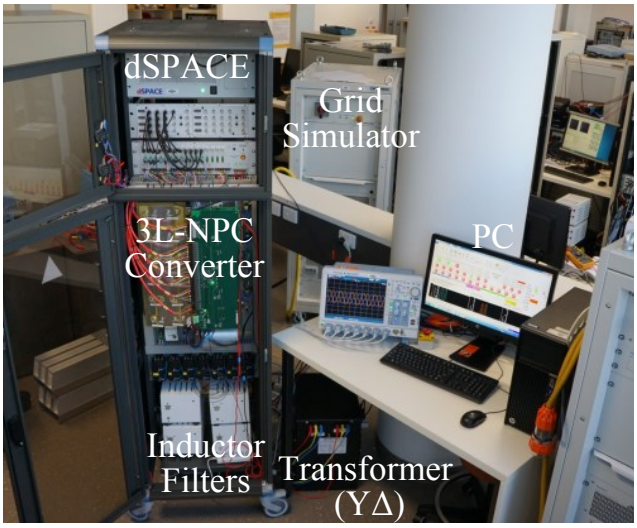

(a)

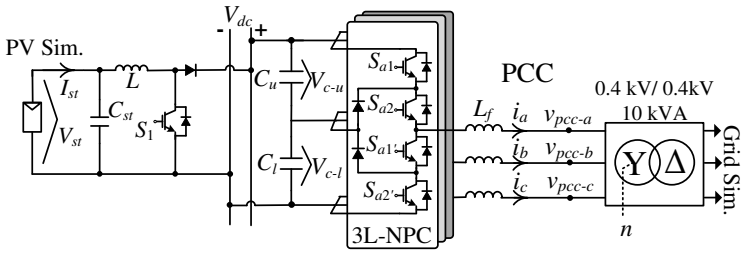

(b)

Fig. 8. *Experimental setup of the grid-connected 3L-NPC inverter: (a) Hardware setup and (b) circuit diagram.*

II, the injected active power is zero and, as a result, the extracted powers from all PV strings are zero.

5. Experimental Validation

A three-phase 3L-NPC converter setup (Fig. 8) has been utilized in order to experimentally validate the effectiveness of the proposed controller under unbalanced voltage sags. The 3L-NPC setup consists of Semikron SKM145GB176D 1700V IGBT modules. The grid is simulated using TopCon TC.ACS 4-quadrant grid simulator while the PV side is emulated using an ETS600/8 Terra SAS photovoltaic simulator and its characteristics are given in Table 1. A dc-dc boost converter is connected between the PV panel and dc-link, which extracts the maximum power for the PV panel during normal operation mode. The proposed controller and protection functions of the converter are implemented in a dSPACE 1006 platform. The parameters of the converter are given in Table 1. The proposed controller has been evaluated under two different cases corresponding to *Sag I* and *Sag II* of Section 4.

Table 1 Experimental Parameters

Parameter	Symbol	Value
PV panel and dc-dc converter parameters		
PV panel maximum power	p_{mpp}	$3.3\,\mathrm{kW}$
PV panel maximum power point voltage	v_{mpp}	$480\,\mathrm{V}$
PV panel maximum power point current	i_{mpp}	$7\,\mathrm{A}$
PV panel filling factor	FF	0.8
PV panel capacitor	C_{pv}	$200\,\mu\mathrm{F}$
dc-dc converter switching frequency	f_{sw}	$10\,\mathrm{kHz}$
3L-NPC inverter parameters		
Apparent power	S	$3.3\,\mathrm{kVA}$
PCC line-to-line voltage	v_{pcc}	$320\,\mathrm{V_{rms}}$
dc-link voltage	V_{dc}	$560\,\mathrm{V_{dc}}$
dc-link capacitor	C_u , C_l	$4.9\,\mathrm{mF}$
Fundamental frequency	f_0	$50\,\mathrm{Hz}$
3L-NPC switching frequency	f_s	$1.5\,\mathrm{kHz}$
Inductor filter	L_f	$4\,\mathrm{mH}$

Sag I It includes 36% two-phase voltage sag for a duration of $150\,\mathrm{ms}$. The three phase grid voltages (v_{pcc}) and injected currents (i_{abc}) are depicted in Fig. 9(a). The amplitude of positive-sequence voltage ($\mid v^{+}_{pcc} \mid$) during *Normal* operation is $270\,\mathrm{V}$ ($1\,\mathrm{pu}$), however it is reduced to $205\,\mathrm{V}$ ($0.77\,\mathrm{pu}$) during *Sag I* mode, as depicted in Fig. 9(b). As a result, k_1 and k_2 changed according to (22) and (23). The value of k_1 increases to 1.02 during the voltage sag, which means P^{+} is larger than P or the amount of negative-sequence active power (P^{-}) is negative, which results in higher injected current (i_c) into the phase with lower voltage ($v_{pcc\text{-}c}$). The dc-link voltage and capacitor voltages are depicted in Fig. 9(b). The dc-link voltage during *Normal* operation is $560\ \mathrm{V_{dc}}$ and is remained constant during *Sag I*. Additionally, dc-link capacitors are remained balanced during all operation modes. The PV voltage (V_{st}) is equal to $480\ \mathrm{V_{dc}}$ during *Normal* mode which shows the operation of the PV string at *MPPT*. During *Sag I*, V_{st} is increased to $555\ \mathrm{V_{dc}}$ through the proposed controller in Fig. 6 in order to decrease the extracted power. The extracted power from PV string (P_{st}) and output current of the PV string (I_{st}) are reduced during *Sag I*.

The quantities of the injected active and reactive powers (p and q) during *Sag I* are illustrated in Fig. 9(c). During *Normal* operation, the 3L-NPC inverter injects purely active power to the grid equal to $3.1\,\mathrm{kW}$. The active power is reduced to $1.3\,\mathrm{kW}$ for the duration of *Sag I*. As expected from the controller, the active power oscillation is zero during *Sag I*. On the other hand, the average of reactive power Q is increased to $2\,\mathrm{kVAR}$. Consequently, the average injected apparent power ($S = \sqrt{1.3^2 + 2^2}$) is equal to $2.4\,\mathrm{kVA}$ which is 77% of the apparent power during *Normal* operation ($S_N = 3.1\ KVA$). It can be seen that the current of the inverter remains within its nominal current.

Sag II It consists of a three-phase voltage sag of 70% as shown in Fig. 10(a). Phase a experiences the smallest voltage amplitude of 30% of the nominal one. Due to the implementation of the proposed controller, the current of phase a is larger than phases b and c during the voltage sag. The dc-link voltage, shown in Fig. 10(b) is remained at its nominal value during *Sag II* while V_{st} is increased to $165\ \mathrm{V_{dc}}$, which is equal to the open-circuit voltage of the PV panel. Accordingly

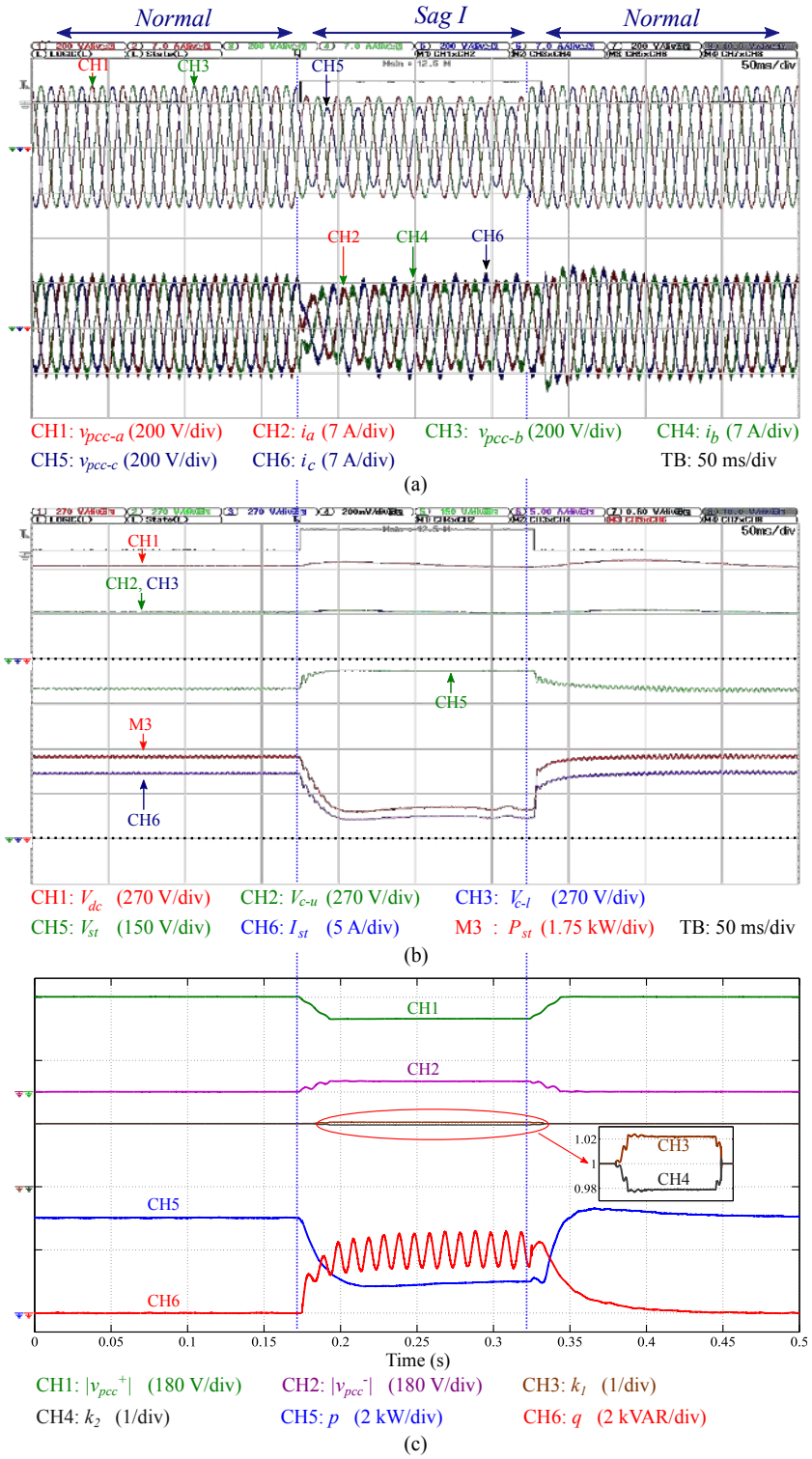

Fig. 9. *Experimental results: Sag I: (a) Three-phase voltage and currents, (b) dc-link voltage, PV string voltage, current and power and (c) positive- and negative-sequence voltages, k_1, k_2 and injected active/reactive power.*

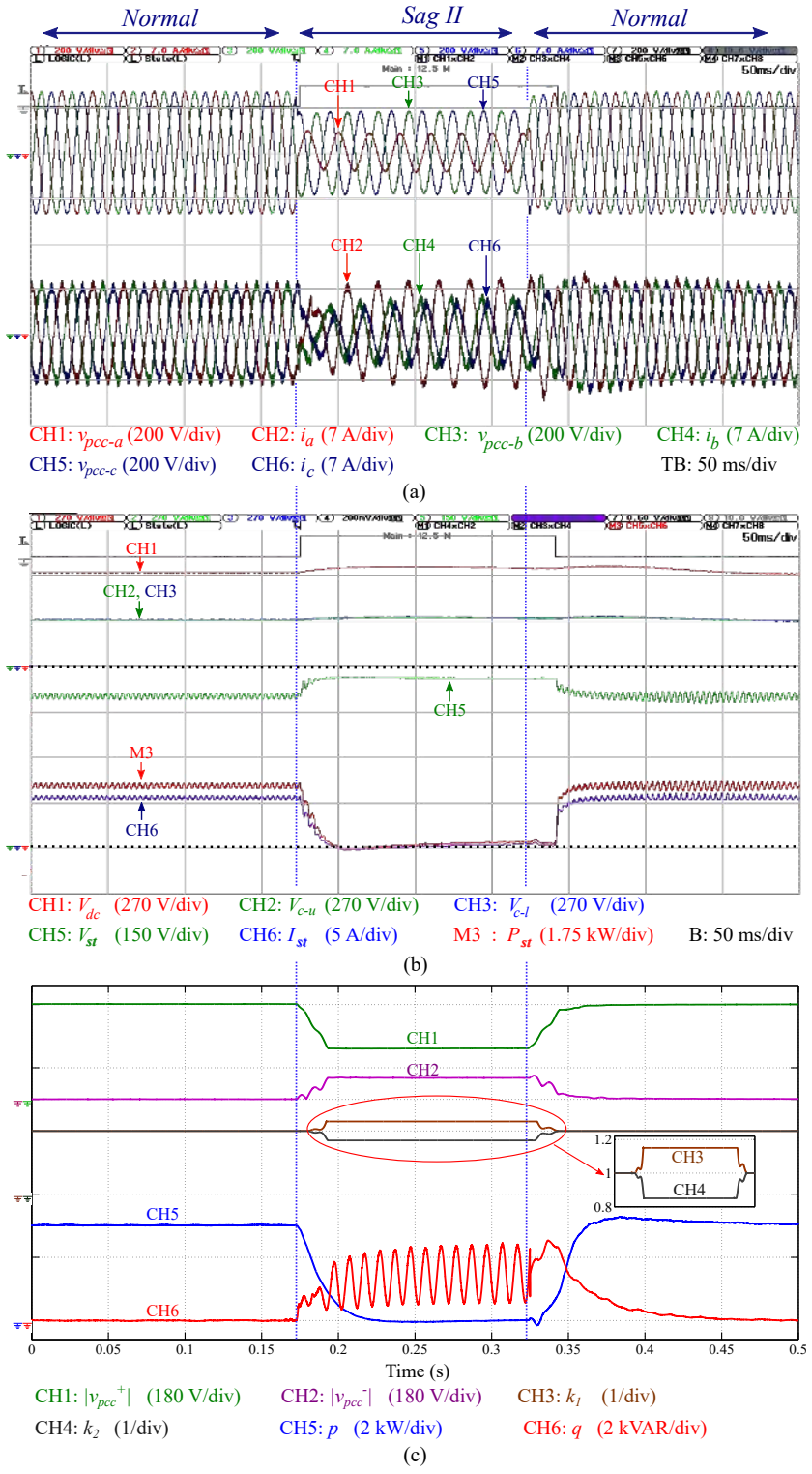

Fig. 10. *Experimental results: Sag II: (a) Three-phase voltage and currents, (b) dc-link voltage, PV string voltage, current and power and (c) positive- and negative-sequence voltages, k_1, k_2 and injected active/reactive power.*

P_{st} and I_{st} are reduced to zero during this condition. The injected active and reactive powers are depicted in Fig. 10(c). It can be seen that p is reduced to zero. The average reactive power (Q) is increased to $1.3\,\mathrm{kVAR}$ during the voltage sag that is 45% of S_N. It should be noted that $\mid v_{pcc}^{+} \mid$ is also reduced to approximately 45% of its nominal value. Therefore, under this condition, the injected reactive power is also reduced to 45% of the nominal apparent power according to (20), which results in remaining the inverter current within its nominal value.

6. Conclusion

A comprehensive control algorithm to limit the inverter peak current and achieve zero active power oscillation for the grid-connected PV power plant (GCPVPP) during unbalanced voltage sags has been introduced and investigated in this paper. The main contribution of this study is to calculate P^* and Q^* as a general equation that can be implemented in combination with various current reference calculation algorithms, while ensures that the inverter peak current remains within its nominal value. Since, the amplitudes of the phase current references depend the voltage positive- and negative-sequences, a rescaling factor (K_{rs}) has been applied in order to ensure the operation of the inverter within its nominal range.

The extracted power from PV strings has been reduced during voltage sags through the implementation of the control algorithm for dc-dc converters of the multi-string GCPVPP. Therefore, the GCPVPP complies with the reactive current requirements of the grid codes and current limitation of the inverter. A detailed implementation of the proposed control scheme has been presented, an its effectiveness has been proved in a 3.3-kVA three-phase grid-connected 3L-NPC inverter prototype. The experimental results verify the theoretical analysis and demonstrate the satisfactory performance of the proposed control algorithm during various voltage sags.

7. References

[1] Bullich-Massague, E., Ferrer-San-Jose, R., Aragues-Penalba, M., *et al.*: 'Power plant control in large-scale photovoltaic plants: design, implementation and validation in a 9.4 MW photovoltaic plant', *IET Renew. Power Gener.*, 2016, **10**, (1), pp 50–62

[2] Yang, Y., Enjeti, P., Blaabjerg, F., *et al.*: 'Wide-scale adoption of photovoltaic energy: grid code modifications are dxplored in the distribution grid', *IEEE Ind. Appl. Mag.*, 2015, **21**, (5), pp 21–31

[3] Camacho, A., Castilla, M., Miret, J., *et al.*: 'Active and reactive power strategies with peak current limitation for distributed generation inverters during unbalanced grid faults', *IEEE Trans. Ind. Electron.*, 2015, **62**, (3), pp 1515–1525

[4] Craciun, B. I., Kerekes, T., Sera, D., *et al.*: 'Frequency support functions in large PV power plants with active power reserves', *IEEE Journal of Emerging and Selected Topics in Power Electron.*, 2014, **2**, (4), pp 849–858

[5] Calle-Prado, A., Alepuz, S., Bordonau, J., *et al.*: 'Model predictive current control of grid-connected neutral-point-clamped converters to meet low-voltage ride-through requirements', *IEEE Trans. Ind. Electron.*, 2015, **62**, (3), pp 1503–1514

[6] Mirhosseini, M., Pou, J., Agelidis, V. G.: 'Single- and two-stage inverter-based grid-connected photovoltaic power plants with ride-through capability under grid faults', *IEEE Trans. Sustain. Energy*, 2015, **6**, (3), pp 1150–1159

[7] Yang, Y., Wang, H., Blaabjerg, F.: 'Reduced junction temperature control during low-voltage ride-through for single-phase photovoltaic inverters', *IET Power Electron.*, 2014, **7**, (8), pp 2050–2059

[8] Camacho, A., Castilla, M., Miret, J., *et al.*: 'Flexible voltage support control for three-phase distributed generation inverters under grid fault', *IEEE Trans. Ind. Electron.*, 2013, **60**, (4), pp 1429–1441

[9] Miret, J., Camacho, A., Castilla, M., *et al.*: 'Control scheme with voltage support capability for distributed generation inverters under voltage sags', *IEEE Trans. Power Electron.*, 2013, **28**, (11), pp 5252–5262

[10] Mirhosseini, M., Pou, J., Agelidis, V. G.: 'Individual phase current control with the capability to avoid overvoltage in grid-connected photovoltaic power plants under unbalanced voltage sags', *IEEE Trans. Power Electron.*, 2015, **30**, (10), pp 5346–5351

[11] Wang, F., Duarte, J. L., Hendrix, M. A. M., *et al.*: 'Design and analysis of active power control strategies for distributed generation inverters under unbalanced grid faults', *IET Gener. Transm. Distrib.*, 2010, **4**, (8), pp 905–916

[12] Rodriguez, P., Timbus, A. V., Teodorescu, R., *et al.*: 'Flexible active power control of distributed power generation systems during grid faults', *IEEE Trans. Ind. Electron.*, 2007, **54**, (5), pp 2583–2592

[13] Wang, F., Duarte, J. L., Hendrix, M. A. M.: 'Active and reactive power control for grid-interactive converters under unbalanced voltage dips', *IEEE Trans. Power Electron.*, 2011, **26**, (5), pp 1511–1521

[14] Sosa, J. L., Castilla, M., Miret, J., *et al.*: 'Control strategy to maximize the power capability of PV three-phase inverters during voltage sags', *IEEE Trans. Power Electron.*, 2016, **31**, (4), pp 3314–3323

[15] Nejabatkhah, F., Li, Y. W., Wu, B.: 'Control strategies of three-phase distributed generation inverters for grid unbalanced voltage compensation', *IEEE Trans. Power Electron.*, 2016, **31**, (7), pp 5228-5241

[16] Miret, J., Castilla, M., Camacho, A., *et al.*: 'Control scheme for photovoltaic three-phase inverters to minimize peak currents during unbalanced grid-voltage sags', *IEEE Trans. Power Electron.*, 2012, **27**, (10), pp 4262–4271

[17] Anurag, A., Yang, Y., Blaabjerg, F.: 'Thermal performance and reliability analysis of single-phase PV inverters with reactive power injection outside feed-in operating hours', *IEEE Journal of Emerging and Selected Topics in Power Electron.*, 2015, **3**, (4), pp 870–880

[18] Castilla, M., Miret, J., Camacho, A., *et al.*: 'Voltage support control strategies for static synchronous compensators under unbalanced voltage sags', *IEEE Trans. Ind. Electron.*, 2014, **61**, (2), pp 808–820

[19] Kabiri, R., Holmes, D. G., McGrath, B. P., *et al.*: 'LV grid voltage regulation using transformer electronic tap changing with PV inverter reactive power injection', *IEEE Journal of Emerging and Selected Topics in Power Electron.*, 2015, **3**, (4), pp 1182–1192

[20] Suul, J. A., Luna, A., Rodriguez, P., *et al.*: 'Virtual-flux-based voltage-sensor-less power control for unbalanced grid conditions', *IEEE Trans. Power Electron.*, 2012, **27**, (9), pp 4071–4087

[21] Lee, C. T., Hsu, C. W., Cheng, P. T.: 'A low-voltage ride-through technique for grid-connected converters of distributed energy resources', *IEEE Trans. Ind. Appl.*, 2011, **47**, (4), pp 1821–1832

[22] Hasanien, H. M.: 'An adaptive control strategy for low voltage ride through capability enhancement of grid-connected photovoltaic power plants', *IEEE Trans. Power Electron.*, 2016, **31**, (4), pp 3230–3237

[23] Kouro, S., Leon, J. I., Vinnikov, D., *et al.*: 'Grid-connected photovoltaic systems: an overview of recent research and emerging PV converter technology', *IEEE Ind. Electron. Magazine*, 2015, **9**, (1), pp 47–61

[24] Ahmed, M. E. S., Orabi, M., Abdelrahim, M.: 'Two-stage micro-grid inverter with high-voltage gain for photovoltaic applications', *IET Power Electron.*, 2013, **6**, (9), pp 1812–1821

[25] IEEE Std 1547-2003: 'IEEE standard for interconnecting distributed resources with electric power systems', 2003

[26] Robles, E., Ceballos, S., Pou, J., *et al.*: 'Variable-frequency grid-sequence detector based on a quasi-Ideal low-pass filter stage and a phase-locked loop', *IEEE Trans. Power Electron.*, 2010, **25**, (10), pp 2552–2563

[27] Mirhosseini, M., Pou, J., Agelidis, V. G., *et al.*: 'A three-phase frequency-adaptive phase-locked loop for independent single-phase operation', *IEEE Trans. Power Electron.*, 2014, **29**, (12), pp 6255–6259

[28] Kabiri, R., Holmes, D. G., McGrath, B. P.: 'Control of active and reactive power ripple to mitigate unbalanced grid voltages', *IEEE Trans. Ind. Appl.*, 2016, **52**, (2), pp 1660–1668

[29] Mirhosseini, M., Pou, J., Karanayil, B., *et al.*: 'Resonant versus conventional controllers in grid-connected photovoltaic power plants under unbalanced grid voltages', *IEEE Trans. Sustainable Enery*, 2016, **7**, (3), pp 1124–1132

[30] Tafti, H. D., Maswood, A., Konstantinou, G., *et al.*: 'Study on the low-voltage ride-thorough capability of photovoltaic grid-connected neutral-point-clamped inverters with active/reactive power injection', *IET Renew. Power Gener.*, 2016, pp 1–9

[31] Debnath, D., Chatterjee, K.: 'Neutral point clamped transformerless grid connected inverter having voltage buck?boost capability for solar photovoltaic systems', *IET Power Electron.*, 2016, **9**, (2), pp 385–392

[32] Tafti, H. D., Maswood, A., Pou, J., *et al.*: 'An algorithm for reduction of extracted power from photovoltaic strings in grid-tied photovoltaic power plants during voltage sags', Proc. IECON 42nd Annual Conf. of the IEEE Industrial Electron. Society, Florence, Italy, 2016, pp 3018–3023